ECOHYDROLOGY
*Ecohydrol.* (2014)
Published online in Wiley Online Library
(wileyonlinelibrary.com) DOI: 10.1002/eco.1477

# Evaluating the use of spatially varying versus bulk average 3D vegetation structural inputs to modelled evapotranspiration within heterogeneous land cover types

G. Sutherland,[1] L. E. Chasmer,[1] R. M. Petrone,[1]* N. Kljun[2] and K. J. Devito[3]

[1] *Department of Geography and Environmental Management, University of Waterloo, Waterloo, Ontario, Canada*
[2] *Department of Geography, Swansea University, Wales, UK*
[3] *Department of Biological Sciences, University of Alberta, Edmonton, Alberta, Canada*

## ABSTRACT

The Western Boreal Plain of north-central Alberta is prone to water-deficit conditions and is hydrologically sensitive to changes in climate, natural resource extraction and disturbance. Accurate measurement and modelling of the main components of the water balance are important for ecosystem and reclamation management; however, the lack of hydro-meteorological instrumentation found within different land cover types makes quantification of changes to the water balance difficult over large areas. Remote sensing data can provide spatial estimates of land cover distribution and leaf area index (LAI) used as inputs into land surface models. However, land surface models can often suffer from inaccuracies as a result of spatial (coarse pixel) and temporal (discrete acquisition) resolutions, mis-classification and inaccurate representation of LAI using remote sensing data. This study uses high-resolution (1 m × 1 m) Light Detection and Ranging-derived vegetation parameters (land cover type, LAI and 3D vegetation frictional influences on air movement) as inputs into the Penman–Monteith evapotranspiration (ET) model along with measured hydro-meteorological variables. Comparison with eddy covariance (EC) measurements indicated that spatially explicit ET estimates at 1 m resolution (over a 5 km × 5 km study area) provided better estimates compared with bulk average ET estimates per land cover type. ET estimates scaled using spatially variable vegetation inputs only underestimated measured fluxes by 2% and 3% at 22·5 and 3 m EC instrumentation towers, respectively. Bulk averaged ET estimates underestimated measured ET by 5% at the 3 m tower and overestimated EC by 7% at the 22·5 m EC tower. Over coarser scales, the error associated with bulk input parameters can lead to error in overall water balance estimation. Copyright © 2014 John Wiley & Sons, Ltd.

KEY WORDS evapotranspiration modelling; LiDAR; eddy covariance; vegetation structure; boreal; wetland; aspen

*Received 12 June 2013; Revised 2 February 2014; Accepted 8 February 2014*

## INTRODUCTION

Evapotranspiration (ET) is often the largest component of the surface energy and water budgets during the growing season in high latitude regions (Comer *et al*., 2000; Cleugh *et al*., 2007; Raddatz *et al*., 2009). Despite its importance to water resources, especially during a changing climate (Brümmer *et al*., 2012), measurements of ET are sparse in these largely inaccessible regions (Zhang *et al*., 2009). The boreal forest covers approximately 58% of Canada and is the largest biome found within these high latitude regions. It also ranges greatly in climate and geology (Anielski and Wilson, 2005). The western boreal plains (WBP) cover 14% of the boreal forest (National Forest Inventory, 2006) and, in contrast with other boreal regions, are undergoing large changes due to industrial development, and oil and gas extraction. ET is particularly important in the WBP, as it often exceeds annual precipitation (P), resulting in frequent water-deficit conditions (Devito *et al*., 2005a), which may be heightened in response to climate warming (Rouse, 1998; Smerdon *et al*., 2005; IPCC, 2007) and rapidly increasing industrial activity.

The WBP is a highly fragmented and heterogeneous landscape (Devito *et al*., 2005b; Brown *et al*., 2010). Many studies (e.g. Avissar and Pielke, 1989; Pickett and Cadenasso, 1995; Smith *et al*. 2003a,2003b; and many others dating back to over a century) have examined the impacts of heterogeneous versus homogeneous land cover types on the ability to classify and adequately quantify earth system processes. Land cover heterogeneity increases with increasingly smaller patch sizes or groupings of similar vegetation species, structural and biophysical attributes, surface hydrology, soil characteristics, biotic/abiotic controls and so on. These may also be described as

Correspondence to: R. M. Petrone, Department of Geography and Environmental Management, University of Waterloo, Waterloo, Ontario, Canada.
E-mail: rich.petrone@uwaterloo.ca

the spatial 'aggregation', 'contagion' or 'patchiness' of a landscape. The heterogeneity of a landscape therefore alters interactions between processes (energy, mass fluxes, ground water movement, infiltration, photosynthesis etc.) at the Earth's surface. Within a remote sensing classification context, increasing fractionation of land cover types can also increase the number of mixed pixels within a land cover classification using remote sensing data. This contributes to further errors in the classification (Muller *et al*. 1998; Smith *et al*. 2003a). When examining surface fluxes of mass and energy exchanges, boundaries between land cover types result in increased roughness lengths (momentum, heat), atmospheric displacement height and greater efficiency of water exchanges between the air–vegetation interface relative to that found in more homogeneous areas (Blonquist *et al*., 2009; Allen *et al*. 2011). The influence of vegetation structure on ET fluxes has been examined in numerous studies (e.g. Baldocchi *et al*. 1991; Kelliher *et al*., 1995; Engel *et al*. 2002; Blonquist *et al*. 2009; Allen *et al*. 2011 Brümmer *et al*. 2012), whereas other studies have modelled the influences of vegetation structure, especially sunlight and shadowed canopies, on ET (e.g. Collatz *et al*. 1991; Chen *et al*. 1999; Dauzat *et al*. 2001; Ge *et al*. 2011). However, to the authors' knowledge, no studies have applied a 3D representation of the vegetation canopy to model ET fluxes.

In landscapes with heterogeneous land cover, such as the WBP, accurate model estimates of ET may improve with spatially explicit measurements of the 3D canopy and understory structure (e.g. vegetation height and leaf area, which both contribute to the surface area available for transpiration), and ground surface elevation and topographic characteristics, which may alter soil moisture regimes. Further, vegetation species types found within land cover classes will also vary leaf stomatal conductance, an important input to ET models. Land cover classes are often derived from spectral remote sensing data and have been used to spatially parameterize ET models along with hydro-meteorological inputs and low-resolution global assimilation data products (e.g. Goddard Earth Observing System Model; e.g. Bastiaanssen *et al*., 1998; Cleugh *et al*., 2007; Zhang *et al*., 2009; Anderson *et al*., 2012). There are, however, several drawbacks for using these inputs within highly heterogeneous regions: (1) inability to resolve landscape heterogeneity within low-resolution pixels (Moran and Jackson, 1991; Kustas *et al*., 2004; Nagler *et al*., 2005; McCabe and Wood, 2006); (2) spectral vegetation indices can saturate at high levels of leaf area index (LAI; Lüdeke *et al*. 1991; Haboudane *et al*., 2004; Wu *et al*., 2008) and can misrepresent ET when applied to multi-layer, densely foliated ecosystems; (3) spectral remote sensing is unable to fully measure the vertical structure of vegetation (Hudak *et al*., 2002); (4) validation of ET estimates derived from low-resolution remote sensing data can be difficult because of the large disparity in scale between *in situ* ET measurements and modelled ET (Li *et al*., 2009); and (5) temporal resolution is reduced as spatial resolution increases, resulting in either wide gaps between data collections (e.g. Landsat – Bastiaanssen *et al*., 1998; Chen *et al*., 2005; Leuning *et al*., 2008; Anderson *et al*., 2012) or low-resolution datasets collected frequently (e.g. MODIS – Cleugh *et al*., 2007; Leuning *et al*., 2008; Ruhoff *et al*., 2012). Higher spatial resolution remote sensing data have been shown to provide more accurate estimates of ET (e.g. McCabe and Wood, 2006; Anderson *et al*., 2012), whereas lower resolution data can lead to increased error (McCabe and Wood, 2006).

The inability to resolve sub-pixel heterogeneity of spaceborne satellite systems may be improved through airborne Light Detection and Ranging (LiDAR) data products. LiDAR measures the 3D canopy, understory and ground surface characteristics at very high spatial resolutions (~0·2 m to several metres; cf., Lim *et al*., 2003; Lefsky *et al*., 2002; Zimble *et al*., 2003). This allows for better separation of the canopy and ground surface (Hopkinson *et al*. 2005) and may be less sensitive to saturation at high LAI (Zhao and Popescu, 2009). Thus, more reliable estimates of canopy geometry and structure can be derived from LiDAR than has been previously possible using spectral remote sensing techniques (Coops *et al*., 2004; Chasmer *et al*., 2008). Airborne LiDAR data are especially useful within heterogeneous areas because of the ability to accurately quantify edges between different land cover types. Large step changes between land cover types (e.g. peatland to riparian buffer zones to mature mixed-wood forests) over relatively short distances create significant changes in the 3D structural properties of vegetation, thereby greatly increasing roughness coefficients at land cover edges and likely significantly altering evaporative fluxes. These 3D structural changes cannot be quantified using spectral data alone, although there exist methods in digital aerial photogrammetry and radar technologies, but often at lower resolutions.

This study combines 1 m × 1 m spatially variable estimates of LAI and canopy height, measured using airborne LiDAR, along with temporally variable wind speed measurements from two representative energy balance instrument towers per land cover type (12 towers in total) to produce maps of zero plane displacement, and roughness lengths for momentum and heat per land cover type across a 5 km × 5 km study area. The purpose of this study is to compare spatially variable zero plane displacement, and roughness lengths for momentum and heat, derived from airborne LiDAR to more frequently used bulk averages per land cover type over a single growing season (1 June to 30 August) in 2008.

## STUDY SITE

The Utikuma Region Study Area (URSA) (56°04′N, 115° 28′W) is located 370 km north of Edmonton (Brown *et al*., 2010) and is approximately 150 km south of the discontinuous permafrost zone (Woo and Winter, 1993). URSA is characterized by cold winters (−16·7 °C mean temperature in January 1970–2000) and warm summers (16·3 °C mean temperature in July 1970–2000) (Devito *et al*., 2005a; Smerdon *et al*., 2005). Long-term (1961–1990) average annual P and PET are 481 mm and 518 mm year$^{-1}$, respectively (Marshall *et al*. 1999), with about 25% (138 mm year$^{-1}$) of the annual P received as snow water equivalent (Ferone and Devito, 2004). More than 60% of P occurs during June to August, resulting in the greatest latent heat fluxes, often followed by a relatively dry autumn (Ferone and Devito, 2004; Devito *et al*., 2005b). For the study period in 2008, the annual rainfall and snowfall were slightly above normal at 504 and 179 mm, respectively. The study period followed 3 years of annual P near or above average, with regional wetting trends in ponds and peatland water levels and soil moisture.

At URSA, quaternary deposits range in depth between 20 and 240 m over Upper Cretaceous Smoky Group shale bedrock (Vogwill, 1978). Glaciofluvial, glaciolacustrine and moraine surficial deposits occur across URSA (Fenton *et al*., 2003). The 5 km × 5 km study area is dominated by moraine deposits, and the ET towers are located on a regional topographic high of a disintegration moraine (Redding and Devito, 2011). Elevation ranges between 650 and 690 m above sea level (Figure 1), whereas local topographic and soil texture differences and associated moisture regimes result in a heterogeneous mosaic of land cover types (Brown *et al*., 2010). Land cover types, percentage coverage within the broader (5 km × 5 km) study area and dominant/sub-dominant vegetation types are summarized in Table I. Peatland soils are comprised of an upper layer of fibric peat (0·3–0·4 m) underlain by mesic peat to a depth of approximately 1·0–1·5 m, with mesic-humified peat extending from 1·5 to 3·5 m (Ferone and Devito, 2004). Feather mosses and sphagnum can be found on high hummocks where sufficient moisture and shelter are offered in riparian zones and treed peatlands (Rydin and Jeglum, 2006). Shallow ponds are underlain by 2–5 m of gyttja (Petrone *et al*., 2007). Near the shore of the pond, submergent macrophyte (*Ceratophyllum demersum*, *Potamogetan richardsoni*, *Potamogetan zosteriformis* and *Myriophyllum exalbescens*), floating macrophyte and emergent graminoids form a buffer between the open water and peatland (Ferone and Devito, 2004). This canopy structure gradient results in rapid changes in aerodynamic roughness over short distances (Petrone *et al*., 2007).

## MEASUREMENTS AND METHODS

### *Hydro-meteorological data collection*

Hydro-meteorological data were averaged over half-hourly periods on north-facing and south-facing slopes (slope angle < 3°) within dominant (classified) land cover types (Figure 1) from 1 June to 30 August 2008 [day of year (DOY) 153–243]. Within each land cover type, two energy balance towers were used to account for within-site variability. Soil moisture ($\Theta$, m$^3$ m$^{-3}$) profiles were measured using water content reflectometry sensors (CS616, Campbell Scientific Inc, Logan, UT, USA) placed at depths of 0·10, 0·30 and 0·50 m below the surface, and calibrated according to Brown *et al*. (2010). Ground temperature ($T_g$, °C) profiles were measured using thermocouples (Omega copper-constantan, Campbell Scientific Inc, Logan, UT, USA) placed at 0·10, 0·25, 0·50 and 1·0 m below the surface. In peatlands and riparian zones, where microtopography was significant, $T_g$ and $\Theta$ were simultaneously measured in hummocks and hollows, and averaged using an aerial weighting.

$T_g$ profiles from each meteorological tower were used to calculate the ground heat flux ($Q_G$) for each site via the calorimetric method (Oke, 1987):

$$Q_G = \Delta Q_{s1} + \Delta Q_{s2} + \cdots + \Delta Q_{sn} + Q_{bottom} \quad (1)$$

where

$$\Delta Q_1 = C_i * \frac{\Delta T_i}{\Delta t} * \Delta z_i \quad (2)$$

and

$$Q_{bottom} = -k_i * \frac{\Delta T_i}{\Delta z_i} \quad (3)$$

where $\Delta Qs_i$ is the change in heat stored in layer $i$ of the soil column, $Q_{bottom}$ is the flux of heat out of the bottom of a 1 m deep soil column, $C_i$ is the heat capacity (MJ m$^{-3}$ K$^{-1}$) of layer $i$ in the soil column, $k_i$ is the thermal conductivity (W m$^{-1}$ K$^{-1}$) of layer $i$, $\Delta T_i$ is the change in temperature (K) across the vertical layer $i$, $\Delta t$ is the change in time (s) over which the measurements were taken and $\Delta z_i$ is the depth (m) of the soil layer $i$ in the soil column.

A water temperature ($T_w$, °C) profile at depths of 0·05, 0·15 and 1·05 m was set up approximately 20 m in-pond from the shore. The $T_w$ sensor at 1·05 m was 0·05 m into the gyttja to account for the flux of energy out of the bottom of the pond. $Q_G$ from ponds was determined using the calorimetric method described earlier.

Air temperature ($T_{air}$, °C) and relative humidity (RH, %) (HOBO Onset Pro Temp/RH, Hoskin Scientific, Vancouver, Canada) were collected at energy balance towers at heights

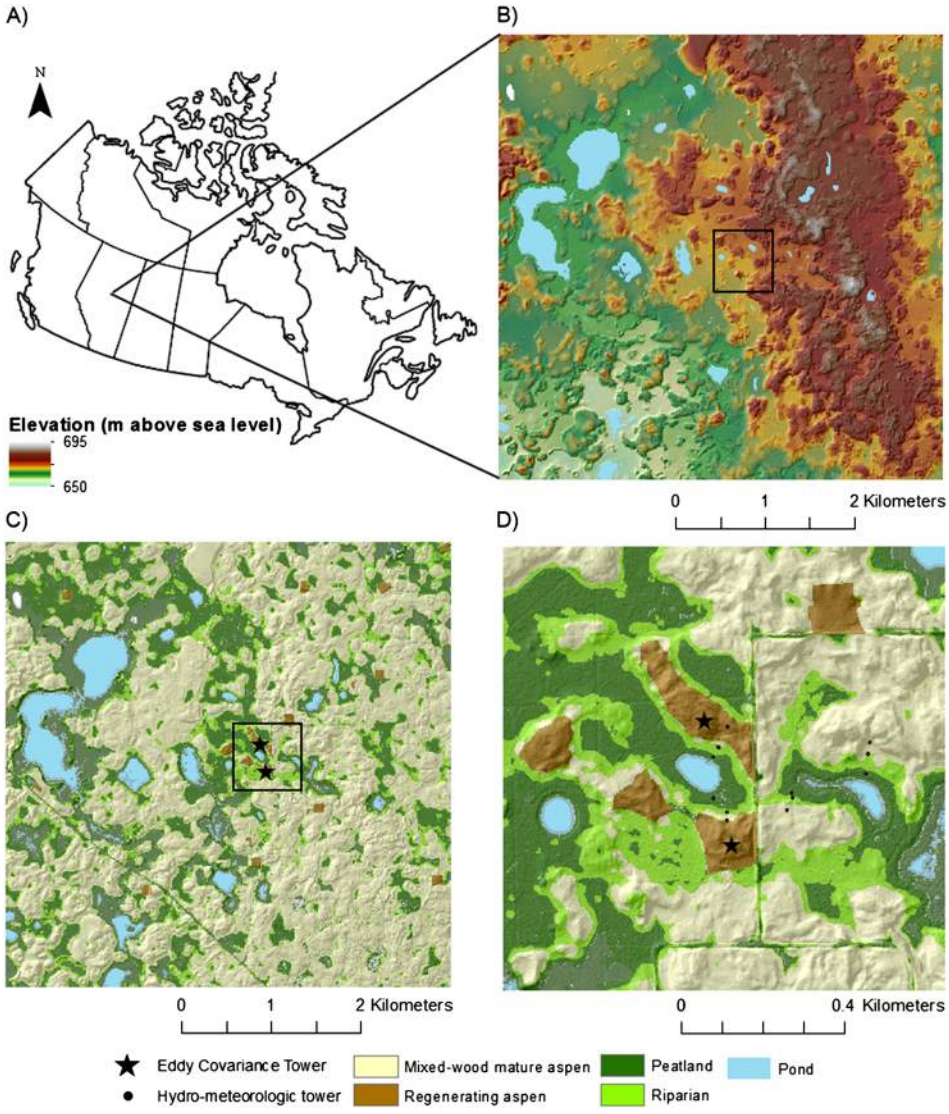


Figure 1. (a) Location of the 5 km × 5 km study site in Canada; (b) DEM derived from LiDAR data of the 5 km × 5 km Utikuma Region Study Area; (c) land cover classification of the study site; and (d) location of energy balance and eddy covariance towers overlain on land cover classification (located in the box in 1b and 1c).

of 1 and 2 m above the ground. Net radiation ($Q^*$, W m$^{-2}$) (NRLite, Kipp and Zonen, The Netherlands) was measured 3 m above the ground. Wind speed ($u$, m s$^{-1}$) and direction (degrees) were measured at heights of 22·5 and 7 m above the surface by an EC system (described later).

Stomatal conductance was measured at individual leaves using a steady state leaf porometer (Model SC-1, Decagon Devices, Inc., Pullman, WA, USA) for species found within the harvested sites (Giroux, 2012). These included aspen, balsam poplar, willow, paper birch, low-bush cranberry and prickly rose (averaged over the growing season for this site). Conductance of individual plants was measured at four heights (apex, 20%, 40% and 60% of total height) per day, along with ambient air temperature, leaf temperature and soil moisture content. Individual leaf undersides were sampled every 10 to 15 days following leaf flush (1 June to 31 August) between 7:30 AM and 4:30 PM (at variable times per day), on sunny days only. Sampling of vegetation did not occur on rainy days or on leaves that were wet. The unit was cleaned daily to remove plant residue.

### *Eddy covariance measurements of ET fluxes and atmospheric stability conditions*

Eddy covariance systems (operating at 20 Hz) measured $H_2O$ fluxes and atmospheric turbulence from two towers. Instrumentation was placed 3 m above ground level within a regenerating aspen stand (harvested in February 2007). A second EC system was installed within a regeneration stand harvested in February 2008, at a height of 22·5 m above the

Table I. Distribution of land cover types applied to the PM model and dominant/sub-dominant species type found within each land cover.

| Land cover type | Percent coverage | Species |
|---|---|---|
| Upland mature mixed-wood | 58 | *Populus tremuloides*, *Populas balsamifera*, *Rosa acicularis* |
| Upland regeneration | 1 | *Populus balsamifera* L., *Salix* spp., *Amelanchier alnifolia*, *Rosa acicularis*, *Viburnum edule*, *Cornus Canadensis*, *Epilobium angustifolium*, *Calamagrostis canadensis* |
| Riparian | 11 | *Populus balsamifera*, *Picea marianca*, *Populus tremuloides*, *Betula papyrifera* |
| Treed peatland | 8 | *Picea marianca*, *Sphagnum* spp. |
| Open peatland | 17 | *Sphagnum* spp. |
| Pond | 5 | See text. |

ground and approximately 7 m above adjacent mature stands. This EC system encompassed a mix of land cover types within the flux footprint and admittedly might be prone to technical limitations of the EC methodology (e.g. Massman and Lee, 2002). Instrumentation included a 3D sonic anemometer (CSAT 3, Campbell Scientific Inc., Edmonton, Alberta, Canada) and an open-path infrared gas analyzer (IRGA) (LI7500, LI-COR Inc., Lincoln, NE, USA). Measurements were averaged every 30 min (Brown *et al*., 2010), and high frequency data were retained for footprint analysis. The IRGA was calibrated according to the Licor Instruction Manual after the 2008 field season and raw fluxes were adjusted if there was any change to calibration coefficients (which was less than 5% of the time). EC data were filtered for periods of low turbulence ($u^* < 0{\cdot}23\,\mathrm{m\,s^{-1}}$ based on the inflection point of $u^*$ in relation to energy balance closure) and corrected for density effects (Webb *et al*., 1980, Leuning and Judd, 1996), coordinate rotation (Kaimal and Finnigan, 1994) and sensor separation (Leuning and Judd, 1996). Approximately 45% of data were lost and gap filled using the mean over 14-day periods (Falge *et al*., 2001).

### *LiDAR data collection and processing*

Light Detection and Ranging data were collected by Alberta Sustainable Resource Development on 20 September 2008 using a small footprint discrete-return ALTM 3100EA (Optech Inc., Toronto, ON, USA) operated at a flying height of 1400 m above ground level. A pulse repetition frequency of 50 kHz and a scan angle of ±25° were employed with 50% overlap between scan lines. This ensured that canopy shadowing was minimal and that both sides of the land surface components would be sampled. The timing of the LiDAR survey corresponded quite closely with end of season foliage senescence. Senescence would be detrimental to this study, if foliage was lost from deciduous vegetation prior to the LiDAR survey. LAI measurements were not collected at the time of the survey; however, an assessment of high temporal resolution Enhanced Vegetation Index (EVI) data from the Moderate resolution Spectroradiometer (MODIS) sensor indicates that for this area, foliage structural changes had not yet occurred, according to the MODIS phenology product (Zhang *et al*. 2003; http://daac.ornl.gov/ accessed on 24 January 2014). Spectral changes in vegetation properties started to change during the 2-week period starting on 13 September. By the week starting on 29 September, lower EVI and likely foliage losses were noticeable. Foliage loss began nearly 1 week following the LiDAR survey; therefore, we assume that canopy foliage was near full foliage conditions during the time of the survey, with minimal leaf loss. Winds during this period were also relatively light and did not exceed speeds of greater than $0{\cdot}89\,\mathrm{m\,s^{-1}}$.

Laser returns were classified into ground, vegetation and all returns using TerraScan (Terrasolid, Finland). A 1 m × 1 m digital elevation model (DEM) was created via an inverse distance weighting approach from ground returns. A canopy height model (CHM) was derived based on the difference between a digital surface model (DSM) (mean maximum height of all returns) and the DEM (Golden Software Surfer, Inc. Golden CO). Gap fraction, determined as the ratio of the total number of returns below 0·5 m (approximate base of the understory) and all returns, was used to estimate effective LAI (Chen *et al*., 2006) using an extinction coefficient of 0·5, and species-specific LAI. Woody-to-total leaf area ratio, needle-to-shoot area ratio and elemental clumping index (described in Chen *et al*., 2006) were determined per land cover dominant species type found within the literature (Table II).

The spatial distribution of land cover types was identified using a decision-tree (Boolean) land cover classification based on airborne LiDAR data. The classification incorporates layers of canopy and understory vegetation structural characteristics associated with land cover types, terrain information and roughness characteristics (e.g. Chasmer *et al*., 2011) (Figure 1c).

### *GIS-based Penman–Monteith model*

The Penman–Monteith (PM) model (Penman, 1948; Monteith, 1965)

Table II. Woody-to-total leaf area ratio ($\alpha$), needle-to-shoot area ratio ($\gamma_E$) and elemental clumping index ($\Omega_E$) used to estimate LAI for dominant vascular vegetation species.

| Species | Woody-to-total leaf area ratio ($\alpha$) | Needle-to-shoot area ratio ($\gamma_E$) | Elemental clumping index ($\Omega_E$) |
|---|---|---|---|
| Poplar | 1 (Pisek *et al*., 2011) | Not required | 0·87 (Pisek *et al*., 2011) |
| Black spruce | 0·12 (Gower *et al*. 1999) | 1·3–1·4 (Gower *et al*. 1999) | 0·7 (Chen *et al*., 1997) |
| Aspen | 0·22 (Gower *et al*. 1999) | Not required | 0·76 (Chen *et al*., 1997) |
| Birch | 0·15 (Ryu *et al*., 2010) | Not required | 0·94 (Ryu *et al*., 2010) |

$$\lambda E = \frac{[\Delta(Q^* - Q_G)] + \rho_a c_p (e_s - e_a)}{\Delta + \Upsilon\left(1 + \frac{r_s}{r_a}\right)} \quad (4)$$

requires temporal inputs of $Q^*$ [net radiation (MJ m$^{-2}$ h$^{-1}$)], $c_p$ [specific heat of the air (KJ kg$^{-1}$ K$^{-1}$)], $Q_G$ [soil heat flux density (MJ m$^{-2}$ h$^{-1}$)], $e_s$ [saturation vapour pressure (kPa)], $e_a$ [actual vapour pressure represented as (kPa)], $\Delta$ [slope vapour pressure curve (kPa °C$^{-1}$)], $\rho_a$ [density of the air (kg m$^{-3}$)], $\Upsilon$ [psychrometric constant (kPa °C$^{-1}$)] and $\lambda$ [latent heat of vaporization (MJ kg$^{-1}$)]. Spatial inputs determined from the LiDAR-derived CHM and LAI per land cover type were used to estimate $r_a$ [aerodynamic resistance (s m$^{-1}$)] and $r_s$ [surface resistance (s m$^{-1}$)], such that

$$r_a = \frac{\ln\left(\frac{z_m - d}{z_{0m}}\right) \ln\left(\frac{z_h - d}{z_{0h}}\right)}{k^2 u_z} \quad (5)$$

and

$$r_s = \frac{r_l}{\mathrm{LAI}} \quad (6)$$

where meteorological inputs to bulk aerodynamic resistance ($r_a$) and bulk surface resistance ($r_s$) include $z_m$ [height of wind measurements (m)], $z_h$ [height of humidity measurements (m)] and $u_z$ [wind speed at height $z_m$ (m s$^{-1}$)], and $k$ is von Karman's constant. LiDAR-derived inputs include $d$ [zero plane displacement (m) at 2/3 height derived from the CHM], $z_0$ and $z_{0h}$ [roughness length governing momentum and heat and water vapour, respectively (m)] (Chasmer *et al*., 2008), and species-specific (classified) LAI (m$^2$ m$^{-2}$). Bulk stomatal resistance ($r_l$, s m$^{-1}$) was determined from porometry measurements and applied to land cover types.

### *Computer model development*

A Python script was created to incorporate bulk hydrometeorological and spatially variable vegetation structural data per land cover type as inputs to the PM model [Equations (4) to (6)] (ESRI, Redlands, CA, USA) (Figure 2). Twenty-four hour mean $e_s$–$e_a$ was compared with 24 h mean VPD to ensure that daily VPD data determined via $e_s$–$e_a$ were representative of the daily mean of half-hourly measured VPD.

The model is driven by average 24 h bulk meteorological inputs and outputs daily, and growing season (cumulative) spatially variable ET maps at 1 m pixel resolution were parameterized for each land cover type. In addition to the spatially variable method, bulk average $r_a$ and $r_s$ terms were applied to determine how well the model corresponds with measured ET if only single (as opposed to spatially variable) inputs are used (Lhomme, 1992; Band, 1993).

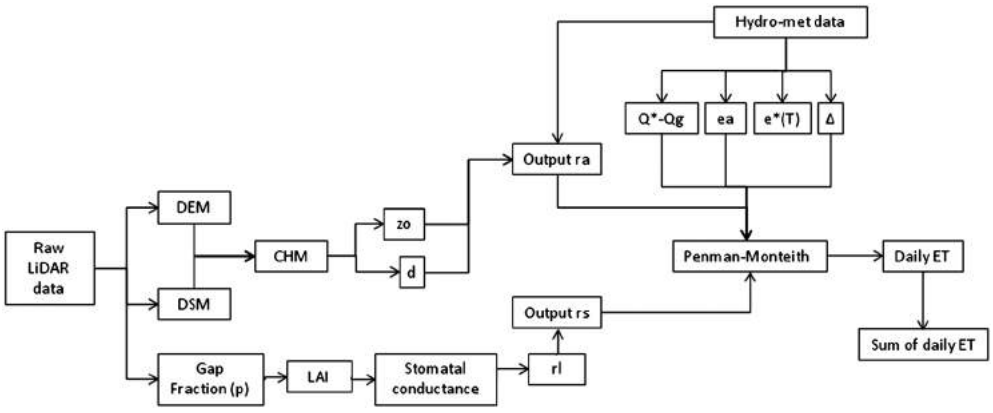


Figure 2. Workflow diagram of the Python-based model in ArcGIS that combines spatially explicit LiDAR-derived canopy structural parameters with measured hydro-meteorological atmospheric and energy drivers of ET via the PM equation.

Statistical analysis was used to determine the variability of modelled ET between land cover types and validation (EC) data. Analysis of variance (ANOVA) tests were used to compare the same variable (e.g. daily ET) across multiple land cover types. When normality tests failed a Kruskal–Wallis, ANOVA on ranks was performed to determine the level of variability between land cover types. In situations when only two groups were being compared (i.e. measured vs modelled ET for a single site), *t*-tests or Mann–Whitney rank sum tests were used when the data were normally distributed or otherwise, respectively. Additional comparisons using linear regression, root mean square error and *p*-statistic from the rank sum, between bulk average versus spatially varying estimates of ET, were used.

### *Flux footprint model*

Spatially varying and bulk averaged methods for estimating ET were compared with EC-derived data via a flux footprint parameterization (Kljun *et al*., 2004) of the approximate daily contribution areas for the fluxes (Chasmer *et al*., 2008; 2011) from 3 and 22·5 m tall EC towers. Flux footprints were calculated every 30 min and accumulated to daily footprints. These were used to estimate the cumulative (weighted) ET within the contribution area (Figure 3). In heterogeneous areas (e.g. URSA), the footprint parameterization provides a rough approximation of the contribution area but is more time efficient than other more complex models [e.g. Lagrangian stochastic particle models (e.g. Kljun *et al*., 2002) or large eddy simulation (Foken and Leclerc, 2004)].

## RESULTS

### *ET regimes of each land cover type*

Modelled spatial estimates of ET, during the period of study, and per land cover type ranged from 150 to 239 mm, with the greatest ET found from riparian areas and lowest ET from mature upland aspen and mixed-wood stands during this study period (Table III; Figure 4). Despite low ET, mixed-wood and aspen uplands had the greatest area extent (58% of the study area) and therefore accounted for 53% of the cumulative ET over the broader study area, whereas riparian zones accounted for 14% of cumulative ET, despite high ET. Regenerating aspen stands, treed peatlands, open peatlands and ponds had higher rates of ET than mixed-wood aspen uplands but only account for 1%, 17%, 9% and 6%, of total ET found within the study region, respectively.

The largest ET rates were found at boundaries between land covers where sharp transitions exist in canopy structure (Figure 4). Spatial variability in ET was greatest in land cover types with a heterogeneous canopy structure (i.e. peatlands and riparian zones), whereas the spatially dominant mixed-wood aspen uplands experienced the lowest spatial variability in ET. Pearson's $r$ correlation coefficient $r = \frac{\mathrm{cov}(x,y)}{\sigma x \cdot \sigma y}$ between the covariance (cov) of spatially variable vegetation and/or topographical influences ($x$) on modelled ET ($y$) divided by their standard deviations, on a per pixel basis, is illustrated in Figure 5. Roughness length [$z_0$ (m)] varies positively with ET, especially in mixed upland sites (to be expected, as $z_0$ is an input to the PM model), whereas the greatest variations

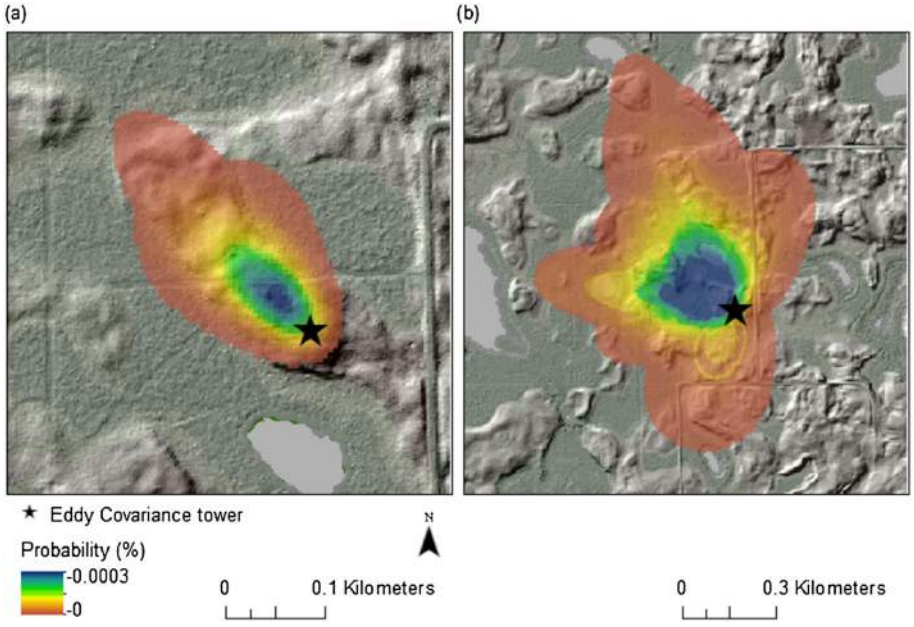


Figure 3. Probability density function showing the percent probability of ET flux contribution from modelled daily flux footprints surrounding the (a) 3 m and (b) 22·5 m eddy covariance towers on DOY 158.

Table III. Cumulative growing season ET estimates from the spatially variable model shown for each land cover type in the 5 km × 5 km study area.

| Land cover | Max cumulative ET (mm) | Min cumulative ET (mm) | Mean cumulative ET (mm) | Average daily ET (mm) | $\sigma$ |
|---|---|---|---|---|---|
| Aspen | 175·3 | 150·5 | 174·5 | 2·0 | ±0·59 |
| Regenerating | 215·7 | 207·9 | 212·2 | 2·4 | ±1·1 |
| Riparian | 239·0 | 236·3 | 237·4 | 2·6 | ±1·3 |
| Treed peatland | 201·2 | 148·0 | 184·1 | 2·1 | ±1·1 |
| Open peatland | 220·5 | 219·2 | 220·0 | 2·4 | ±1·2 |
| Water | N/A | N/A | 209·8 | 2·3 | ±1·3 |

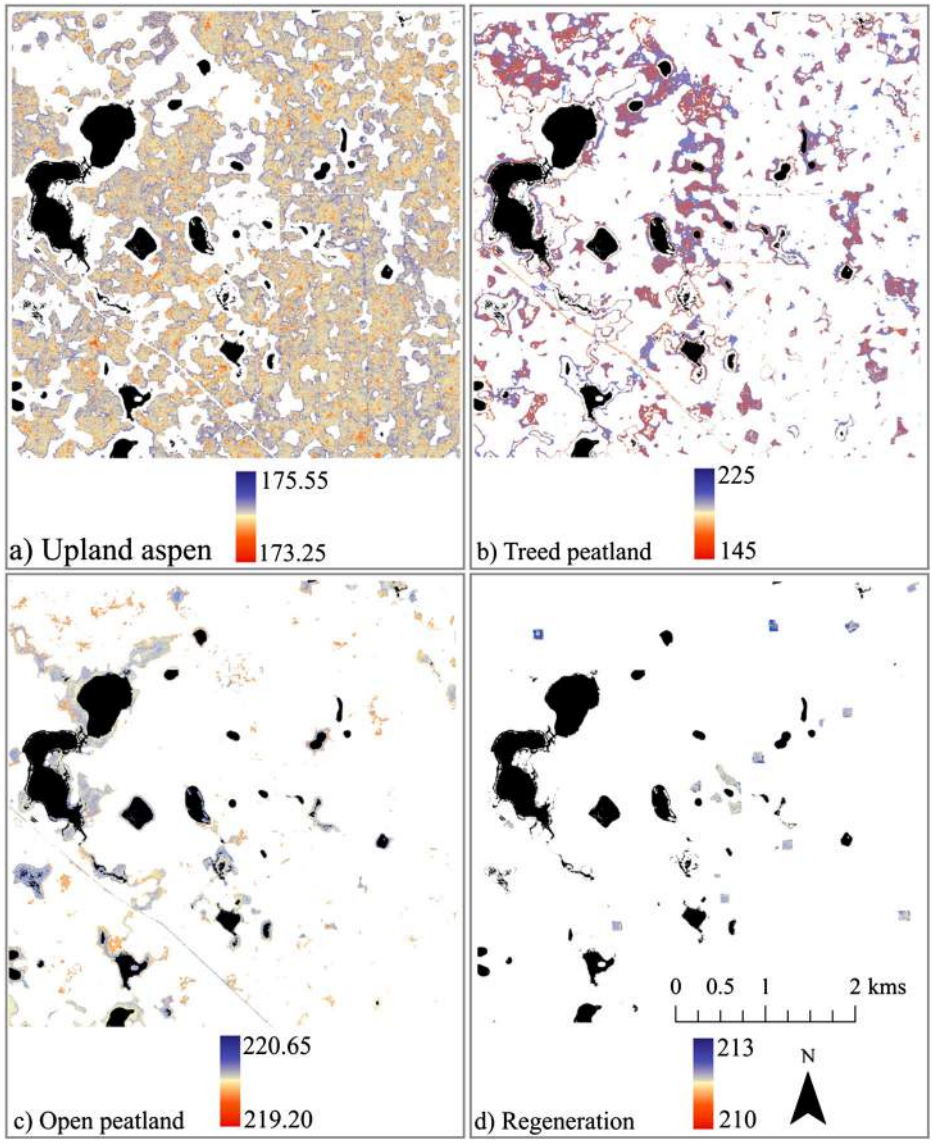


Figure 4. 1 m × 1 m resolution spatially explicit cumulative ET estimates for (a) mixed-wood aspen uplands, (b) treed peatlands, (c) open peatlands and (d) regenerating aspen stands.

occur at the edges of land cover types and negatively in peatlands where vegetation structure is not measured by airborne LiDAR. Gap fraction, including understory (which contributes to aerodynamic resistance, surface resistance and stomatal conductance inputs), was negatively correlated with ET in upland aspen and regenerating aspen stands, but positively correlated within peatlands. Elevation and the canopy height above a topographically varying ground surface (DSM) were not highly correlated with modelled ET.

Petrone *et al.* (2007) showed lower peatland ET rates, because of drought conditions and low water levels in peatlands (which may break the capillary fringe) early in the decade. However, in 2008, with higher water levels, ponds and peatlands may remove (ET) more than P. Model results show Aspen ET is lower for the centres of stands, but the edges mix with riparian; thus, the total Aspen ET may be higher. For this period, the middle of aspen stands remove 92% of P (Table III).

Spatially variable estimates of daily ET reached a maximum of 5·2 mm on 5 June (DOY 157) over open water and a minimum of −0·4 mm on 26 June (DOY 178) also over open water (Figure 6). All land cover types experienced a similar temporal trend in ET with peak ET rates in the early part of the growing season along with peaks in measured $Q^*$, water availability and atmospheric

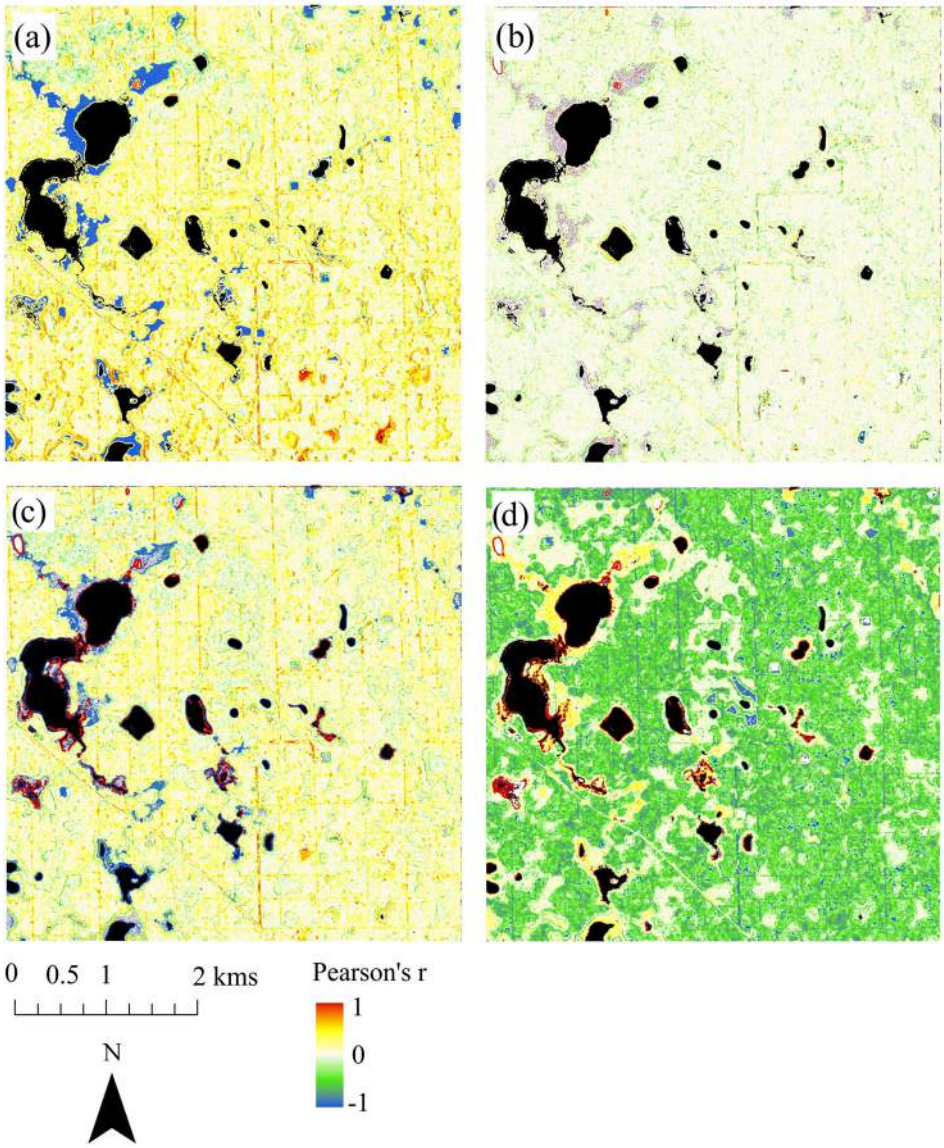


Figure 5. Pearson's *r* correlation coefficient (0 to 1 = positive correlation; 0 to −1 = negative correlation) between modelled ET and (a) roughness length [$z_0$ (m)]; (b) elevation (normalized to remove underlying topographic trend); (c) canopy height over variable topography; and (d) gap fraction of canopy and understory vegetation. Black areas indicate water.

demand for water. Bulk estimates of daily ET consistently overestimated spatially variable estimates of daily ET over the study period in treed peatlands and riparian zones while underestimating spatially variable daily ET in mature forests, regenerating forests and open peatlands (Figure 7; Table IV).

Peaks in ET following P events occurred within 3 days depending on how shortly after the P events' energy inputs increased (i.e. cloud cover dissipation). ET in riparian zones and ponds had the most pronounced response within 3 days following P events in June and July, whereas in July and August, all land cover types showed similar responses to P. For all land cover types, peaks in ET following P events were short lived (1–2 days).

### *Validation of PM model outputs*

The dominant wind direction for the 22·5 m EC tower was between 220 and 280°, within which approximately 60% of the land area covered by the flux footprint was mixed-wood aspen upland, 13% peatland, 10% pond, 12% riparian and 5% regenerating aspen. In the early half of the study period, unstable atmospheric conditions resulted in smaller flux footprints originating from variable wind directions,

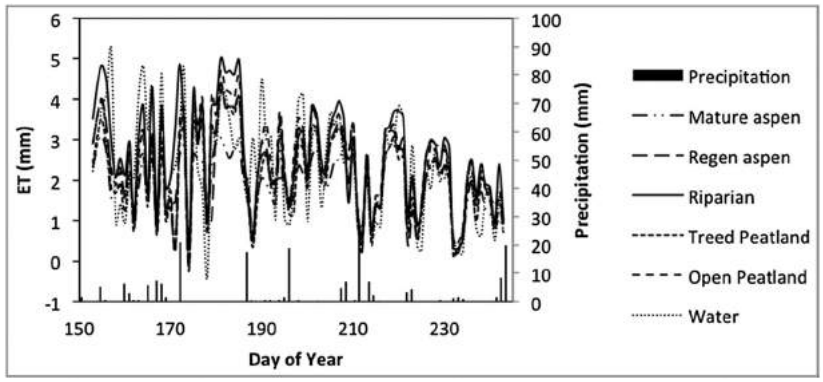


Figure 6. ET estimated for each land cover type using the spatially variable model.

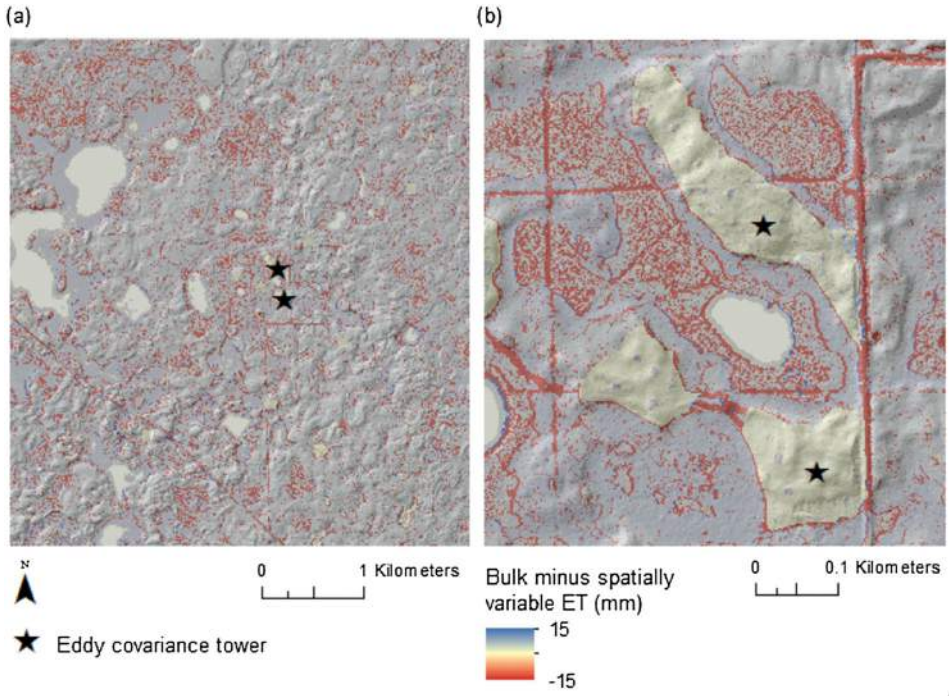


Figure 7. Spatial differences in ET estimated using the bulk average method relative to the spatially variable method for (a) the entire study site and (b) the area surrounding the eddy covariance towers. Blue areas show where the bulk model overestimates spatially variable ET, and red areas show where the bulk model underestimates spatially variable ET.

Table IV. Average difference (mm) and range of differences in daily values of ET as seen between ET estimated with bulk land cover inputs and ET estimates based on spatially variable land cover inputs.

| Land cover | Mean difference (mm) | $\sigma$ | Average daily range of differences (mm) | Significant difference ($P < 0{\cdot}05$)? |
|---|---|---|---|---|
| Aspen | −0·1 | ±0·3 | ±0·2 | No |
| Regenerating | −0·1 | ±1·4 | ±3·0 | No |
| Riparian | 3·0 | ±0·1 | ±6·0 | No |
| Treed peatland | 15·0 | ±2·0 | ±4·0 | Yes |
| Open peatland | −2·0 | ±0·1 | ±1·5 | No |

whereas more stable atmospheric conditions promoted larger flux footprints in the middle-to-late portion of the study period, generally occurring from the dominant wind direction (220–280°).

Spatially variable ET extracted from flux footprints showed good agreement with EC fluxes at the 22·5 m tower (~2% underestimation; Table V). No significant differences (Mann–Whitney rank sum, $P > 0{\cdot}05$) were found between the spatially variable model and EC fluxes at the daily or weekly time scale (Figure 8). Bulk ET estimates extracted from the same footprint overestimated seasonal ET by ~7% at the 22·5 m tower (Table V); however, no significant differences (Mann–Whitney rank sum, $P > 0{\cdot}05$) were observed at the daily or weekly time scale. Because of EC measurements with $z_m$ within the roughness sublayer being disregarded, the flux footprint model at the 3 m EC tower was only run for 34 of 90 days (38%) with dominant wind direction from the northwest (300–340°). Spatially variable ET slightly underestimated EC fluxes by ~3% (Table V), and no significant differences (Mann–Whitney rank sum, $P > 0{\cdot}05$) were found at the daily or weekly time scales. Bulk ET estimates underestimated EC fluxes by ~5% (Table V) also with no significant differences (Mann–Whitney rank sum, $P > 0{\cdot}05$) at the daily or weekly time scales.

Table V. Accuracy of ET modelled using spatially variable and spatially averaged input parameters relative to ET modelled from 22·5 and 3 m eddy covariance towers.

| Input data | Modelled ET (mm) | Percent difference (%) | Significant difference ($P < 0{\cdot}05$)? | $r^2$ | RMSE |
|---|---|---|---|---|---|
| Spatially variable versus 22·5 m EC | 185 | −2 | No | 0·58 | 1·14 |
| Spatially averaged versus 22·5 m EC | 202 | 7 | No | 0·62 | 1·21 |
| Spatially variable versus 3 m EC | 64 | −3 | No | 0·85 | 0·17 |
| Spatially averaged versus 3 m EC | 63 | −5 | No | 0·80 | 0·36 |

RMSE, root mean square error.

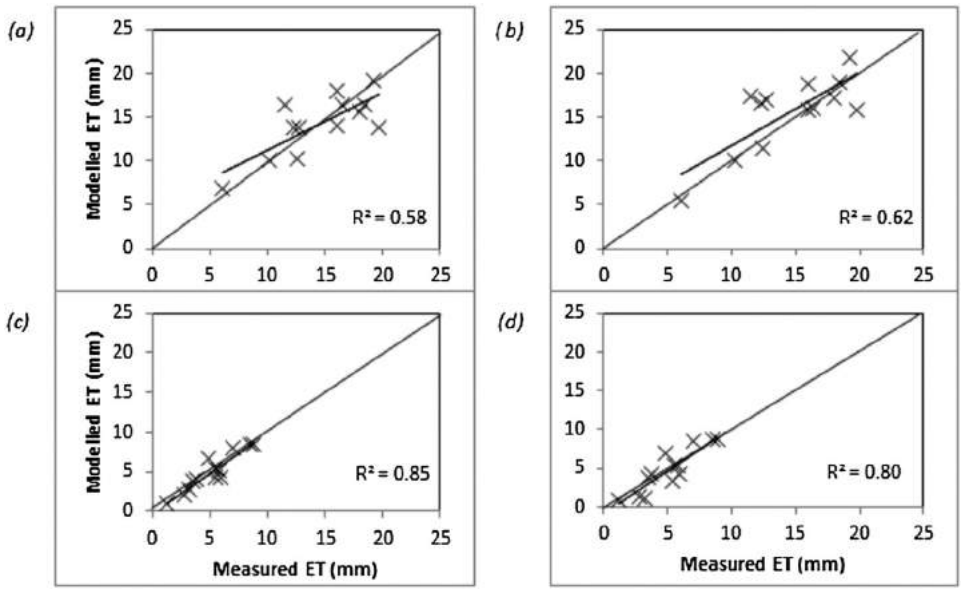


Figure 8. Correlation between weekly eddy covariance ET data and modelled ET extracted from flux footprints at various EC towers: (a) spatially variable ET versus 22·5 m EC tower (RMSE = 1·14 mm week$^{-1}$); (b) spatially averaged ET versus 22·5 m EC tower (RMSE = 1·21 mm week$^{-1}$); (c) spatially variable ET versus 3 m EC tower (0·17 mm week$^{-1}$); and (d) spatially averaged versus 3 m EC tower (0·36 mm week$^{-1}$).

## DISCUSSION

### *ET between land cover types*

Differences in ET amongst different land cover types are due in part to different responses of vascular and non-vascular vegetation to drivers of ET ($Q^*$, VPD, $g_s$ etc.). Land cover types with vascular vegetation showed an increase in stomatal resistance in response to midday peaks in VPD resulting in reduction of afternoon transpiration rates. Conversely, in land cover types dominated by non-vascular vegetation (i.e. open peatlands), *Sphagnum* rely on surface wicking and capillary action to transport water (Rydin and Jeglum, 2006); therefore, it is surface resistance, rather than stomatal resistance, that dictates the rate of water vapour exchange between vegetation and the atmosphere when water is available (Admiral and Lafleur, 2007). As a result, peak daytime and peak season increases in VPD over non-vascular vegetation and open water promote enhanced ET in response to the atmospheric gradient if adequate $\Theta$ is present (Admiral *et al*., 2006; Raddatz *et al*., 2009).

Transpiration from land cover types dominated by vascular vegetation (mixed-wood upland aspen, regenerating uplands, treed peatlands and riparian zones) is limited by stomatal closure. For example, open and treed peatlands had comparable energy inputs, soil moisture levels and VPD, but open peatlands had a total growing season ET 38·2 mm higher than treed peatlands. Because vegetation in open peatlands lack stomatal control and have a large surface area, they experience high rates of ET (Heijmans *et al*., 2004).

This study occurred during a wetter cycle over the past decade and water levels, and thus, availability, in peatlands, is high and not limited as in other periods (Petrone *et al*. 2007). The modelled aspen ET is lower in this study than for other boreal aspen studies (Amiro *et al* 2006, Zha *et al*. 2010), but the estimates here are somewhat biassed for centre of stands, as the edges are classified and included in the riparian estimates, which may show higher values (Chasmer *et al*. 2011). In drier climatic conditions, aspen ET will exceed that of the peatlands. However, in this study, aspen stands still consume 92% of P, whereas Brown *et al*. (2013) found that 88 ± 1% and 75 ± 2% of P was used for evaporation processes within the same stand, through the late spring and summer months in 2005 and 2006. They also found that 15 ± 0·5% (2005) and 12 ± 0·2% (2006) of P was intercepted by the canopy.

In all land cover types, daytime ET was strongly tied to $Q^*$ and $Q^*$–$Q_G$ (e.g. Admiral *et al*., 2006), whereas night-time ET was a function of atmospheric VPD and wind. Ponds exhibited the consistently largest $Q_G$ because of the high heat capacity of water (Oke, 1987) causing larger storage of energy within the water column (e.g. Chapin *et al*., 2002; Petrone *et al*., 2007; Granger and Hedstrom, 2011) and slower responses of ET to fluctuations in $Q^*$ (Oke, 1987). The lag time between peak energy inputs and peak energy storage in ponds results in energy being released later in the growing season (Granger and Hedstrom, 2011) when open water bodies become warm relative to cooling atmospheric temperatures (Chapin *et al*., 2002). This can promote sustained water losses from open water bodies compared with terrestrial wetland and forestland cover types.

### *ET between models and EC towers*

Variability in land cover composition has been shown to influence the accuracy of modelled fluxes relative to EC estimates when scaling fluxes to broader areas (Soegaard *et al*., 2000; Kim *et al*., 2006; Göckede *et al*., 2008; Chen *et al*., 2011; Gelybó *et al*., 2013). In this study, standard deviations of ±0·8 mm day$^{-1}$, or ~40% of average daily ET, were associated with the flux footprint from the 3 m tower, whereas standard deviations of ±1 mm day$^{-1}$, or ~50% of average daily ET, were associated with the flux footprint from the 22·5 m tower.

Better agreement was found between modelled estimates of ET (both bulk averaged and spatially variable) and EC-derived estimates at the 3 m tower as opposed to the 22·5 m tower. This is because the flux footprint surrounding the 3 m tower was restricted to a relatively homogeneous land cover of regenerating aspen uplands and sampled fluxes near the tops of short, regenerating vegetation. The footprint extended beyond the regeneration stand into the surrounding mature aspen uplands ~40% of the study period; however, the greatest probability of flux contribution remained within the regenerating stand ~90% of the study period. This indicates that homogeneous areas can be adequately represented by either the spatially variable model or the bulk average model. However, at the 22·5 m EC tower, the flux footprint extends hundreds of metres into unequally weighted land cover types, resulting in variable contributions of water fluxes to the EC system and also to the PM outputs (Figure 3), causing an increased deviation of bulk ET estimates from EC data.

Errors in bulk average ET estimates more than double that of spatially variable ET estimates in areas where there are large canopy gaps (exceeding one 1 m × 1 m pixel). These differences occur because the bulk average model estimates ET for every pixel within each land cover class using the same average canopy structural inputs. Therefore, bulk average methods do not account for gaps within the canopy and assume total foliage coverage, thereby increasing the surface area for ET fluxes. However, in the spatially variable ET example, openings in the canopy are void of structural information and therefore have much lower rates of modelled evaporation, based only on the soil surface. Whether this is actually the case in these environments at the time of study has not been quantified beyond comparisons with EC data and flux footprints. Consequently, whereas bulk ET estimates are accurate in land cover types that do not vary greatly in vegetation structural characteristics, they are less reliable in land covers that are highly heterogeneous.

This is particularly evident in bulk average model output for treed peatlands, which experience an overestimation of

ET. This uncertainty propagates into flux footprint validations when treed peatlands are present. In this study, the area of maximum flux contribution for the 3 m EC tower extended into treed peatlands ~10% of the study period. Consequently, bulk ET and spatially variable ET both estimate EC data comparably well. However, the area of maximum flux contribution for the 22·5 m EC tower extended into treed peatlands for ~75% of the study period. In this case, misrepresentations in vegetation structure (and thus ET) associated with the bulk model contaminate the larger flux footprint and make this method three times less accurate than the spatially variable ET model. Consequently, when upscaling from tens to hundreds of metres over heterogeneous land covers and canopy structures, the agreement between EC data and ET modelled using bulk vegetation inputs declines, and there is a marked advantage in utilizing spatially explicit model inputs of vegetation structure.

The bulk averaging procedure may be useful for the removal of outliers in ET estimates (Bian and Butler, 1999), thereby smoothing spatial data. However, edge influences, which can often be very important to landscape scale ET, may be missed (e.g. Petrone *et al*. 2007). For example, step changes at land cover boundaries may increase atmospheric drag and roughness length (McAneney *et al*. 1994 Loranty *et al*. 2010; Brümmer *et al*. 2012), depending on the adjacent land cover type and the vegetation structural attributes. Use of bulk averages may underestimate the influence of vegetation structural variability on roughness and ET fluxes (Klaassen and Claussen, 1995; De Jong *et al*., 1999) especially for aspen stands that frequently occur on crests of hummocks, and the edges may represent areas of larger ET. Such underestimations may impede our ability to predict the response of these regions' ecohydrological processes to climatic variability and landuse change, both of which are significant stresses in the WBP.

## CONCLUSIONS

In order for ET estimates to be scaled beyond the flux footprint of the EC system, detailed information on the structure of vegetation governing ET is required. In this study, high-resolution LiDAR data products of vegetation structural characteristics were used to derive spatially variable estimates of ET compared with land cover-based bulk averages within the heterogeneous WBP. These were then compared with ET estimates from the EC method at heights of 3 and 22·5 m above a naturally regenerating aspen stand and a mixture of land cover types (respectively).

Estimates of spatially variable ET were in better agreement with validation at both the 3 and 22·5 m tall towers, whereas ET estimates derived from land cover-based bulk average vegetation inputs did not correspond as well with validation, particularly when scaled to the landscape scale. This study illustrates the importance of high-resolution vegetation frictional inputs to the PM model in heterogeneous areas that are sensitive to small changes in the local climate and water balance.

Landuse and climatic changes could lengthen the growing season and increase ET fluxes in this region. This may further reduce current water resources and increase water deficit conditions, especially where it already exceeds P inputs. Prolonged deficits can impact the seasonal course of water cycling, plant growth and carbon uptake (Kljun *et al*., 2007; Brümmer *et al*., 2012). Such information is integral to the management of ecosystem services and water resources in climatically and hydrologically sensitive areas such as the WBP, which are also subject to intensive industrial activity that impacts the landscape scale. Because ET in the WBP is the dominant hydrological flux, understanding the controls on that flux at the regional scale is vital to the ability to predict the ecohydrological response of this region to further disturbance.

## ACKNOWLEDGMENTS

The authors would like to thank the anonymous reviewers of this manuscript. Their insightful comments have helped to make this a much-improved work. The authors would like to thank Mr S. Brown for his technical assistance in the field. Funding for this work was provided by an NSERC Discovery Grant (Petrone), NSERC Collaborative Research and Development Grant (HEAD2) (Devito, Petrone), NSERC Research Tools and Instrument Grant (Petrone) and the Cumulative Environmental Managers Association (CEMA).

## REFERENCES

Admiral SM, Lafleur PM, Roulet NT. 2006. Controls on latent heat flux and energy partitioning at a peat bog in eastern Canada. *Agricultural and Forest Meteorology* **140**: 308–321.

Admiral SM, Lafleur PM. 2007. Partitioning of latent heat flux at a northern peatland. *Aquatic Botany* **86**: 107–116.

Allen RG, Pereira LS, Howell TA, Jensen ME. 2011. Review: evapotranspiration information reporting: 1. Factors governing measurement accuracy. *Agricultural Water Management* **98**: 899–920.

Amiro, BD, Barr, AG, Black TA, Iwashita H, Kljun N, McCaughey JH, Morganstern K, Murayama S, Nesic Z, Orchansky AL, Saigusa N. 2006. Carbon, energy and water fluxes at mature and disturbed forest sites, Saskatchewan, Canada. *Agricultural Forest Meteorology*, **136**: 151–168.

Anderson MC, Allen RG, Morse A, Kustas WP. 2012. Use of Landsat thermal imagery in monitoring evapotranspiration and managing water resources. *Remote Sensing of Environment* doi:10.1016/j.rse.2011.08.025.

Anielski M, Wilson S. 2005. Counting Canada's capital: assessing the real value of Canada's boreal ecosystems. The Canadian Boreal Initiative. Accessed: http://www.borealcanada.ca/ documents/Boreal_Wealth_Report_Nov_2005_000.pdf.

Avissar R, Pielke RA. 1989. A parameterization of heterogeneous land surfaces for atmospheric numerical models and its impact on regional meteorology. *Monthly Weather Review* **117**(10): 2113–2136.

Band LE. 1993. Effect of land surface representation on forest water and carbon budgets. *Journal of Hydrology* **150**: 749–772.

Baldocchi DD, Luxmoore RJ, Hatfield JL. 1991. Discerning the forest from the trees: an essay on scaling canopy stomatal conductance. *Agricultural and Forest Meteorology* **54**: 197–226.

 

Bastiaanssen WGM, Menenti M, Feddes RA, Holtslag AAM. 1998. A remote sensing surface energy balance algorithm for land (SEBAL): part 1 formulation. *Journal of Hydrology* **212–213**: 198–212.

Bian L, Butler R. 1999. Comparing effects of aggregation methods on statistical and spatial properties of simulated spatial data. *Photogrammetric Engineering & Remote Sensing* **65**(1): 73–84.

Blonquist Jr. JM, Norman JM, Bugbee B. 2009. Automated measurement of canopy stomatal conductance based on infrared temperature. *Agricultural and Forest Meteorology* **149**: 1931–1945.

Brown SM, Petrone RM, Mendoza C, Devito KJ. 2010. Surface vegetation controls on evapotranspiration from a sub-humid Western Boreal Plain wetland. *Hydrological Processes* **24**: 1072–1085.

Brown SM, Petrone RM, Chasmer L, Mendoza C, Lazerjan MS, Landhäuser SM, Silins U, Leach J, Devito KJ. 2013. Atmospheric and soil moisture controls on evapotranspiration from above and within a Western Boreal Plain aspen forest. *Hydrological Processes*. DOI: 10.1002/hyp.9879.

Brümmer, C, TA Black, RS Jassal, NJ Grant, DL Spittlehouse, B Chen, Z Nesic, BD Amiro, MA Arian, AG Barr, CP-A Bourque, C Courselle, AL Dunn, LB Flanagan, ER Humphreys, PM Lafleur, HA Margolis, JH McCaughey, SC Wofsy. 2012. How climate and vegetation type influence evapotranspiration and water use efficiency in Canadian forest, peatland and grassland ecosystems. *Agricultural and Forest Meteorology* **153**: 14–30.

Chapin FS, Matson PA, Mooney HA. 2002. *Principles of Terrestrial Ecosystem Ecology*. New York: Springer. ISBN 0-387-95443-0.

Chasmer L, Hopkinson C, Treitz P, McCaughey H, Barr A, Black TA. 2008. A lidar-based hierarchical approach for assessing MODIS fPAR. *Remote Sensing of Environment* **112**: 4344–4357.

Chasmer L, Kljun N, Hopkinson C, Brown S, Milne T, Giroux K, Barr A, Devito K, Creed I, Petrone RM. 2011. Characterizing vegetation structural and topographic characteristics sampled by eddy covariance within two mature aspen stands using lidar and a flux footprint model: scaling to MODIS, *Journal of Geophysical Research* **116**: G02026, doi:10.1029/2010JG001567.

Chen B, Coops NC, Fu D, Margolis HA, Amiro BD, Barr AG, Black TA, Arain MA, Bourque CP-A, Flanagan LB, Lafleur PM, McCaughey JH, Wofsy SC. 2011. Assessing eddy-covariance flux tower location bias across the Fluxnet-Canada Research Network based on remote sensing and footprint modelling. *Agricultural and Forest Meteorology* doi:10.1016/j.agrformet.2010.09.005.

Chen JM, Liu J, Cihlar J, Goulden ML. 1999. Daily canopy photosynthesis model through temporal and spatial scaling for remote sensing applications. *Ecological Modelling* **124**: 99–119.

Chen JM, Chen X, Ju W, Geng X. 2005. Distributed hydrological model for mapping evapotranspiration using remote sensing inputs. *Journal of Hydrology* **305**: 15–39.

Chen JM, Govind A, Sonnentag O, ZhangY, BA, Amiro B. 2006. Leaf area index measurements at Fluxnet-Canada forest sites. *Agricultural and Forest Meteorology* **140**: 257–268. doi:10.1016/j.agrformet.2006.08.005.

Chen JM, Rich PM, Gower ST, Norman JM, Plummer S. 1997. Leaf area index of boreal forests: theory, techniques, and measurements. *Journal of Geophysical Research-Atmospheres* **102**: 29429–29443.

Cleugh HA, Leuning R, Mu Q, Running SW. 2007. Regional evaporation estimates from flux tower and MODIS satellite data. *Remote sensing of Environment* **106**: 285–304.

Collatz GJ, Ball JT, Grivet C, Berry JA. 1991. Physiological and environmental regulation of stomatal conductance, photosynthesis and transpiration: a model that includes a laminar boundary layer. *Agricultural and Forest Meteorology* **54**: 107–136.

Comer NT, Lafleur PM, Roulet NT, Letts MG, Skarupa M, Verseghy D. 2000. A test of the Canadian Land Surface Scheme (CLASS) for a variety of wetland types. *Atmosphere Ocean* **38**: 161–179.

Coops NC, Wulder MA, Culvenor DC, St-Onge B. 2004. Comparison of forest attributes extracted from fine spatial resolution multi-spectral and LiDAR data. *Canadian Journal of Remote Sensing* **30**:855–866.

Dauzat J, Rapidel B, Berger A. 2001. Simulation of leaf transpiration and sap flow in virtual plants: model description and application to a coffee plantation in Costa Rica. *Agricultural and Forest Meteorology* **109**: 143–160.

De Jong JJM, De Vries AC, Klaassen W. 1999. Influence of obstacles on the aerodynamic roughness length of the Netherlands. *Boundary Layer Meteorology* **91**: 51–64.

Devito KJ, Creed IF, Fraser CJD. 2005a. Controls on runoff from a partially harvested aspen-forested headwater catchment, Boreal Plain, Canada. *Hydrological Processes* **19**: 3–25.

Devito KJ, Creed IF, Gan T, Mendoza C, Petrone RM, Silins U, Smerdon B. 2005b. A framework for broad-scale classification of hydrologic response units on the Boreal Plain: is topography the last thing to consider? *Hydrological Processes* **19**: 1705–1714.

Engel VC, Stieglitz M, Williams M, Griffin KL. 2002. Forest canopy hydraulic properties and catchment water balance: observations and modeling. *Ecological Modelling* **154**: 263–288.

Falge E, Baldocchi D, Olson R, Anthoni P, Aubinet M, Bernhofer C, Burba G, Ceulemans R, Clement R, Dolman H, Granier A, Gross P, Grünwald T, Hollinger D, Jensen N-O, Katul G, Keronen P, Kowalski A, Lai CT, Law BE, Meyers T, Moncrieff J, Moors E, Munger JW, Pilegaard K, Rannick Ü, Rebmann C, Suyker A, Tenhunen J, Tu K, Verma S, Vesala T, Ilson K, Wofsy S. 2001. Gap filling strategies for long term energy flux data sets. *Agricultural and Forest Meteorology* **107**: 71–77.

Fenton MM, Paulen RC, Pawlowicz JG. 2003. *Surficial Geology of Lubicon Lake Area, Alberta (NTS 84B/SW)*. Alberta Geological Survey: Edmonton.

Ferone J-M, Devito KJ. 2004. Shallow groundwater–surface water interactions in pond–peatland complexes along a Boreal Plain topographic gradient. *Journal of Hydrology* **292**: 75–95.

Foken T, Leclerc MY. 2004. Methods and limitations in validation of footprint models, *Agricultural and Forest Meteorology* **127**: 223–234.

Ge Z-M, Zhou X, Kellomäki S, Peltola H, Wang K-Y. 2011. Climate, canopy conductance and leaf area development controls on evapotranspiration in a boreal coniferous forest over a 10-year period: a united model assessment. *Ecological Modelling* **222**: 1626–1638.

Gelybó GZ, Barcza A, Kern N, Kljun N. 2013. Effect of spatial heterogeneity on the validation of remote sensing based GPP estimations. *Agricultural and Forest Meteorology* **174–175**: 43–53.

Giroux K. 2012. Pre- and post-harvest carbon dioxide fluxes from an upland boreal aspen (*Populus tremuloides*) forest in Western Boreal Plain, Alberta, Canada. Master's Thesis. Wilfrid Laurier University.

Göckede M, Foken T, Aubinet M, Aurela M, Banza J, Bernhofer C, Bonnefond JM, Brunet Y, Carrara A, Clement R, Dellwik E, Elbers J, Eugster W, Fuhrer J, Granier A, Grünwald T, Heinesch B, Janssens IA, Knohl A, Koeble R, Laurila T, Longdoz B, Manca G, Marek M, Markkanen T, Mateus J, Matteucci G, Mauder M, Migliavacca M, Minerbi S, Moncrieff J, Montagnani L, Moors E, Ourcival J-M, Papale D, Pereira J, Pilegaard K, Pita G, Rambal S, Rebmann C, Rodrigues A, Rotenberg E, Sanz MJ, Sedlak P, Seufert G, Siebicke L, Soussana JF, Valentini R, Vesala T, Verbeeck H, Yakir D. 2008. Quality control of CarboEurope flux data – part 1: coupling footprint analyses with flux data quality assessment to evaluate sites in forest ecosystems. *Biogeosciences* **5**: 433–450.

Gower ST, Kucharik CJ, Norman JM. 1999. Direct and indirect estimation of leaf area index, fAPAR, and net primary production of terrestrial ecosystems. *Remote Sensing of Environment* **70**: 29–51.

Granger RJ, Hedstrom N. 2011. Modelling hourly rates of evaporation from small lakes. *Hydrology and Earth System Sciences* **15**: 267–277.

Haboudane D, Miller JR, Pattey E, Zarco-Tejada PJ, Strachan IB. 2004. Hyperspectral vegetation indices and novel algorithms for predicting green LAI of crop canopies: modeling and validation in the context of precision agriculture. *Remote Sensing of Environment* **90**(3): 337–352.

Heijmans MMPD, Arp WJ, Chapin II FS. 2004. Controls on moss evaporation in a boreal black spruce forest. *Global Biogeochemical Cycles* **18**: GB2004, doi:l0.1029/2003GB002128.

Hopkinson C, Chasmer LE, Sass G, Creed IF, Sitar M, Kalbfeisch W, Treitz P. 2005. Vegetation class dependent errors in lidar ground elevation and canopy height estimates in a boreal wetland environment. *Canadian Journal of Remote Sensing* **31**(2): 191–206.

Hudak AT, Lefsky MA, Cohen WB, Berterretche M. 2002. Integration of lidar and Landsat ETM + data for estimating and mapping forest canopy height. *Remote Sensing of Environment* **82**: 397–416.

IPCC. 2007. *Contribution of Working Group II to the Fourth Assessment Report of the Intergovernmental Panel on Climate Change*, Parry ML, Canziani OF, Palutikof JP, PJ van der Linden, CE Hanson (eds) Cambridge University Press: Cambridge, United Kingdom and New York, NY, USA.

Kaimal JC, Finnigan J. 1994. *Atmospheric Boundary Layer Flows: Their Structure and Measurement*. Oxford Univ. Press: New York; 255–261.

 

Kelliher FM, Leuning R, Raupach MR, Schulze E-D. 1995. Maximum conductances for evaporation from global vegetation types. *Agricultural and Forest Meteorology* **73**: 1–16.

Kim J, Guo Q, Baldocchi DD, Leclerc M, Xu L, Schmid HP. 2006. Upscaling fluxes from tower to landscape: overlaying flux footprints on high-resolution (IKONOS) images of vegetation cover. *Agricultural and Forest Meteorology* **136**: 132–146.

Klaassen W, Claussen M. 1995. Landscape variability and surface flux parameterization in climate models. *Agricultural and Forest Meteorology* **73**: 181–188.

Kljun N, Rotach MW, Schmid HP. 2002. A 3D backward Lagrangian footprint model for a wide range of boundary layer stratifications. *Boundary-Layer Meteorology* **103**: 205–226.

Kljun N, Calanca P, Rotach MW, Schmid HP. 2004. A simple parameterisation for flux footprint predictions. *Boundary-Layer Meteorology* **112**: 503–523.

Kljun N, Black TA, Griffis TJ, Barr AG, Gaumont-Guay D, Morgenstern K, McCaughey JH, Nesic Z. 2007. Response of net ecosystem productivity of three boreal forest stands to drought. *Ecosystems* **9**: 1128–1144.

Kustas WP, Li F, Jackson TJ, Prueger JH, MacPherson JI, Wolde M. 2004. Effects of remote sensing pixel resolution on modeled energy flux variability of croplands in Iowa. *Remote Sensing of Environment* **92**(4): 535–547.

Lefsky MA, Cohen WB, Parker GG, Harding DJ. 2002. Lidar remote sensing for ecosystem studies. *Bioscience* **52**(1): 19–30.

Leuning R, Judd MJ. 1996. The relative merits of open and closed path analysers for measurement of eddy fluxes. *Global Change Biology* **2**: 241–253.

Leuning R, Zhang YQ, Rajaud A, Cleugh H, Tu K. 2008. A simple surface conductance model to estimate regional evaporation using MODIS leaf area index and the Penman–Monteith equation. *Water Resources Research* **44**: W10419, doi:10.1029/2007WR006562.

Lhomme JP. 1992. Energy balance of heterogeneous terrain: averaging the controlling parameters. *Agricultural and Forest Meteorology* **61**: 11 21.

Li Z-L, Tang R, Wan Z, Bi Y, Zhou C, Tang B, Yan G, Zhang X. 2009. A review of current methodologies for regional evapotranspiration estimation from remotely sensed data. *Sensors* **9**: 3801–3853.

Lim K, Treitz P, Wulder M, St-Onge B, Flood M. 2003. LiDAR remote sensing of forest structure. *Progress in Physical Geography* **27**(1): 88–106.

Loranty MM, Mackay DS, Ewers BE, Traver E, Kruger EL. 2010. Competition for light between individual trees lowers reference canopy stomatal conductance: results from a model. *Journal of Geophysical Research* **115**: G04019, doi:10.1029/2010JG001377.

Lüdeke M, Janecek A, Kohlmaier GH. 1991. Modelling the seasonal CO2 uptake by land vegetation using the global vegetation index. *Tellus* **43B**: 188–196.

Marshall IB, Schut P, Ballard M (compilers). 1999. Canadian ecodistrict climate normals for Canada 1961–1990. A national ecological framework for Canada: attribute data. Environmental Quality Branch, Ecosystems Science Directorate, Environment Canada and Research Branch, Agriculture and Agri-Food Canada, Ottawa/Hull.

Massman WJ, Lee X. 2002. Eddy covariance flux corrections and uncertainties in long-term studies of carbon and energy exchange. *Agricultural and Forest Meteorology* **113**: 121–144.

McAneney KJ, Brunet Y, Itier B. 1994. Downwind evolution of transpiration by two irrigated crops under conditions of local advection. *Journal of Hydrology* **161**: 375–388.

McCabe MF, Wood EF. 2006. Scale influences on the remote estimation of evapotranspiration using multiple satellite sensors. *Remote Sensing of Environment* **105**: 271–295.

Monteith, JL. 1965. Evaporation and environment. In *Symposium of the Society for Experimental Biology, The State and Movement of Water in Living Organisms*, Fogg GE (ed.) Vol. **19**. Academic Press, Inc.: NY; 205–234.

Moran MS, Jackson RD. 1991. Assessing the spatial distribution of evapotranspiration using remotely sensed inputs. *Journal of Environmental Quality* **20**: 725–737.

Muller SV, Walker DA, Nelson FE, Auerbach NA, Brockheim JG, Guyer S, Sherba D. 1998. Accuracy assessment of a land-cover map of the Kuparuk River Basin, Alaska: considerations for remote regions. *Photogrammetric Engineering and Remote Sensing* **64**(6): 619–628.

Nagler Cleverly PJ, Glenn E, Lampkin D, Huete A, Wan Z. 2005. Predicting riparian evapotranspiration from MODIS vegetation indices and meteorological data. *Remote Sensing of Environment* **94**: 17–30.

National Forest Inventory. 2006. Accessed June 2011 from: http://nfi.nfis.org.

Oke TR. 1987. Boundary layer climates. Methuen & Co, Ltd.

Penman HL. 1948. Natural evaporation from open water, bare soil and grass. Proc. Roy. Soc. London A(194), S. 120–145.

Petrone RM, Silins U, Devito KJ. 2007. Dynamics of evapotranspiration from a riparian pond complex in the Western Boreal Forest, Alberta, Canada. *Hydrological Processes* **21**: 1391–1401.

Pickett STA, Cadenasso ML. 1995. Landscape ecology: spatial heterogeneity in ecological systems. *Science* **269**(5222): 331–334.

Pisek J, Chen JM, Nilson T. 2011. Estimation of vegetation clumping index using MODIS BRDF data. *International Journal of Remote Sensing* **32**(9): 2645–2657.

Raddatz RL, Papakyriakou TN, Swystun KA, Tenuta M. 2009. Evapotranspiration from a wetland tundra sedge fen: surface resistance of peat for land-surface schemes. *Agriculture and Forest Meteorology* **149**: 851–861.

Redding TE, KJ Devito. 2011. Aspect and soil texture control of snowmelt runoff on forested Boreal Plain hillslopes. *Hydrology Research* **42**(4): 250–267.

Rouse WR. 1998. A water balance model for a subarctic sedge fen and its application to climatic change. *Climate Change* **38**: 207–234.

Ruhoff LA, Paz AR, Collishonn W, Aragao LEOC, Rocha HR, Malhi YS. 2012. A MODIS-based energy balance to estimate evapotranspiration for clear-sky days in Brazilian tropical savannas. *Remote Sensing* **4**: 703–725.

Rydin H, Jeglum JK. 2006. *The Biology of Peatlands*. Oxford University Pres.: New York.

Ryu Y, Nilson T, Kobayashi H, Sonnentag O. 2010. On the correct estimation of effective leaf area index: Does it reveal information on clumping effects?. *Agricultural and Forest Meteorology* **150**: 463–472.

Smerdon BD, Devito KJ, Mendoza CA. 2005. Interaction of groundwater and shallow lakes on outwash sediments in the subhumid Boreal Plains region. *Journal of Hydrology* **314**: 246–262.

Smith JH, Wickham JD, Stehman SV, Yang L. 2003a. Impacts of patch size and land-cover heterogeneity on thematic image classification accuracy. *Photogrammetric Engineering and Remote Sensing* **68**(1): 65–70.

Smith JH, Stehman SV, Wickham JD, Yang L. 2003b. Effects of landscape characteristics on land-cover class accuracy. *Remote Sensing of Environment* **84**(3): 342–349.

Soegaard H, Nordstroem C, Friborg T, Hansen BU, Christensen BR, Bay C. 2000. Trace gas exchange in a high arctic valley 3. Integrating and scaling CO2 fluxes from canopy to landscape using flux data, footprint modeling and remote sensing. *Global Biochemical Cycles* **14**: 725–744.

Vogwill RIJ. 1978. Hydrogeology of the Lesser Slave Lake area, Alberta. Alberta Research Council.

Webb EK, Pearman G, Leuning R. 1980. Correction of flux measurements for density effects due to heat and water vapour transfer. *Quarterly Journal of the Royal Meteorology Society* **106**: 85–100.

Woo M-K, Winter TC. 1993. The role of permafrost and seasonal frost in the hydrology of northern wetlands in North America. *Journal of Hydrology* **141**: 5–31.

Wu CY, Niu Z, Tang Q, Huang W. 2008. Estimating chlorophyll content from hyperspectral vegetation indices: modeling and validation. *Agricultural and Forest Meteorology* **148**(8–9): 1230–1241.

Zhang K, Kimball JS, Mu Q, Jones LA, Goetz SJ, Running SW. 2009. Satellite based analysis of northern ET trends and associated changes in the regional water balance from 1983 to 2005. *Journal of Hydrology* **379**: 92–110.

Zhang X, Friedl MA, Schaaf CB, Strahler AH, Hodges JCH, Gao F, Reed BC, Huete A. 2003. Monitoring vegetation phenology using MODIS. *Remote Sensing of Environment* **84**(3): 471–475.

Zhao K, Popescu S. 2009. Lidar-based mapping of leaf area index and its use for validating GLOBCARBON satellite LAI product in a temperate forest of the southern USA. *Remote Sensing of Environment* **113**: 1628–1645.

Zha T, Barr AG, van der Kamp G, Black TA, McCaughey JH, Flanagan L. 2010. Interannual variation of evapotranspiration from forest and grassland ecosystems in Western Canada in relation to drought. *Agricultural and Forest Meteorology* **150**(11): 1476–1484.

Zimble DA, Evans DL, Carlson GC, Parker RC, Grado SC, Gerard PD. 2003. Characterizing vertical forest structure using small-footprint airborne LiDAR. *Remote Sensing of Environment* **87**: 171–182.

 